JOURNAL OF Materials CHEMISTRY

A new form of oxygen deficient 1201-cobaltite $(Tl_{0.4}Sr_{0.5}Co_{0.1})Sr_2CoO_{5-\delta}$: structure, transport and magnetic properties

A. Maignan, D. Pelloquin, C. Martin, M. Hervieu and B. Raveau

Laboratoire CRISMAT, UMR CNRS ISMRA 6508, 6 bd Maréchal Juin, 14050 Caen Cedex, France

Received 14th September 2001, Accepted 23rd January 2002
First published as an Advance Article on the web 4th March 2002

The investigation of the Tl–Sr–Co–O system has allowed a new form of 1201-type cobaltite to be synthesized. The HREM study of this oxide, $Tl_{0.4}Sr_{2.5}Co_{1.1}O_{5-\delta}$ ($\delta \approx 0.20$) shows that it consists of an association, in the same matrix, of two phasoïds, the tetragonal oxygen stoichiometric 1201-structure $Tl_{0.4}Sr_{2.5}Co_{1.1}O_5$ ($a \approx a_{1201}$, $c \approx c_{1201}$) and a new ordered oxygen deficient 1201 $Tl_{0.4}Sr_{2.5}Co_{1.1}O_{4.5}$ ($a \approx 2a_{1201}$, $b \approx a_{1201}$ $c \approx 2c_{1201}$). The latter is described as the intergrowth of double rock salt layers $[Sr_{1.5}Tl_{0.4}Co_{0.1}O_2]_\infty$ with single ordered oxygen deficient perovskite layers $[SrCoO_{2.5}]_\infty$ similar to $YBaFeCuO_5$. The magnetic and transport properties of this Sr-rich oxide differ fundamentally from the 1201 cobaltite $TlSr_2CoO_5$, by the absence of a metal to insulator transition as a function of temperature. The as-synthesized sample exhibits a semiconducting and paramagnetic behavior down to 50 K, with $\theta_p = -160$ K indicative of antiferromagnetic correlations. The oxygen pressure annealed sample shows a much lower resistivity, T independent down to 200 K, and weak ferromagnetism in agreement with its θ_p value (+50 K). These properties and thermopower measurements are interpreted on the basis of Co^{4+} carriers in an intermediate spins Co^{3+} matrix.

I. Introduction

Oxides represent a huge source for the generation of new properties as recently shown with the discovery of superconductivity at high temperature in cuprates and of colossal magnetoresistance in manganites. In this respect cobalt oxides are also promising candidates for transport, magnetic and thermal properties. For instance, the $LaCoO_3$ perovskite exhibits a thermally induced spin-state transition from low-spin Co(III) to high-spin Co^{3+}.[1] Upon substitution of divalent strontium for trivalent lanthanum, this compound evolves from a semiconducting paramagnetic to a metallic ferromagnet[2] connected with magnetoresistance properties.[3,4] Trivalent cobalt in the one-dimensional oxide, $Ca_3Co_2O_6$, sets in alternating CoO_6 octahedra and trigonal prisms[5] to form ferromagnetic chains which are antiferromagnetically coupled.[6,7] These chains are an experimental realization of an Ising triangular lattice.[8] In $Ca_3Co_2O_6$, the abrupt changes in magnetization induced by the magnetic field are interpreted by different possible arrangements of the magnetic moments of the chains on the Co hexagonal array. Recently, in the 2D metallic mixed-valent cobaltite $NaCo_2O_4$, within which the edge-shared CoO_6 octahedra form CdI_2 type layers interleaved with partially filled sodium layers,[9] a large room temperature thermopower has been reported.[10] So the search for new thermoelectric materials based on metal–transition oxides is a very active field. The large thermopower in $NaCo_2O_4$ and in 'misfit' cobaltites[11,12] is ascribed to the low spin-states configurations of trivalent and tetravalent cobalt cations that form a 2D triangular lattice. A last example is given by the metal–insulator (M-I) transitions at about 300 K that are coupled to magnetic transitions in both the oxygen-deficient perovskite $LnBaCo_2O_{5.5}$ (Ln = lanthanides), which crystallizes in the '112' structure,[13] and the thallium strontium cobaltite, $TlSr_2CoO_5$, analogous to the '1201' cuprate, made of intergrowths of double rock salt type layers with single octahedral cobalt layers derived from the perovskite.[14,15] Both cobalt oxides contain mainly trivalent cobalt and their M-I transition is attributed to a spin-state transition.

The 1201-type structure is of interest, due to its great flexibility, which allows large variations of cationic compositions and oxygen non-stoichiometry, as shown recently for $(Bi_{0.5}Sr_{0.5})Sr_2CoO_{5-\delta}$[16] in which the main structural feature deals with the Bi/Sr cationic ordering in the centre of the block of rock salt type layers. Such phenomena are thought to influence the transport and magnetic properties of these oxides. For these reasons we have revisited the Tl–Sr–Co–O system studying the possibility of generating a mixed $[(Tl/Sr)O]_\infty$ layer in a 1201 cobaltite.

We report herein on a new Sr-rich 1201-type, $(Tl_{0.4}Sr_{2.5}Co_{0.1})$-$Sr_2CoO_{5-\delta}$ which structure, although closely related to that of stoichiometric $TlSr_2CoO_5$,[14,15,17,18] differs from the latter by the existence of a mixed [(Tl,Co,Sr)O] layer. In the following, the synthesis, the structural features established by transmission electron microscopy (TEM) and powder X-ray diffraction (XRD) and the physical properties investigated by means of magnetism, resistivity and thermopower measurements of this oxygen-deficient thallium-based 1201 cobaltite are reported and discussed.

II. Experimental

In contrast to the experimental process given for the synthesis of $TlSr_2CoO_5$,[17] no preliminary precursor, such as $Sr_2Co_2O_{10}$, has been used. All samples have been prepared in a one step reaction from a mixture of Tl_2O_3, SrO/SrO_2 and Co_3O_4 oxides weighted in the proportions according to the formula $Tl_{0.5-x}Sr_{2.5+x}CoO_{5-\delta}$. The mixtures, intimately ground in an agate mortar and pressed in the form of bars, were placed in an alumina crucible. Note that nominal oxygen stoichiometry was controlled through the ratio SrO_2 : SrO and that the weighing and preparation of the bars was carried out in a dry box. Then, the mixtures were sealed in an evacuated

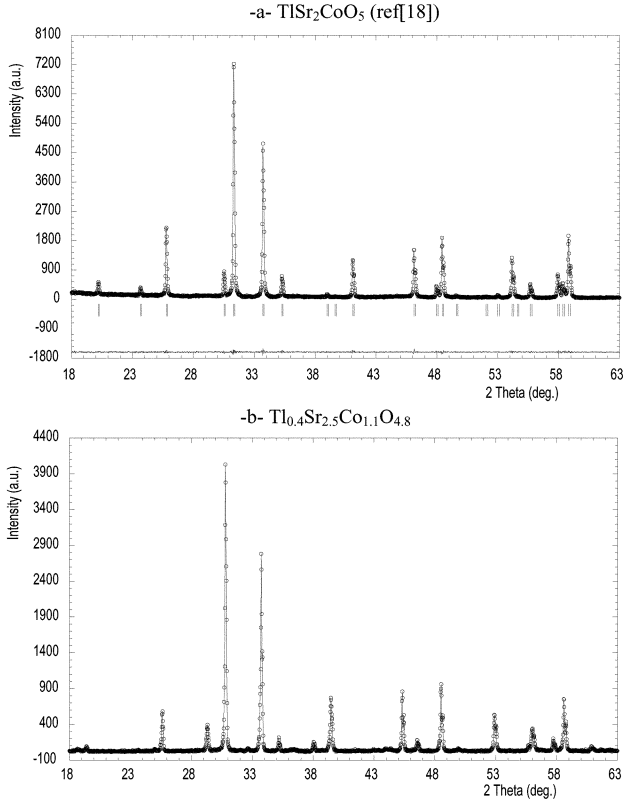

Fig. 1 X-ray diffraction patterns of (a) $TlSr_2CoO_5$ (simulated from structural data given in ref. 18) and (b) $Tl_{0.4}Sr_{2.5}Co_{1.1}O_{4.8}$.

quartz tube and heated up to 1000 °C at 150 °C h^{-1}, kept at this temperature for 2 h and quenched to room temperature. The oxygen content was estimated by chemical analysis using redox titrations. The preliminary electron diffraction (ED) studies were carried out using a JEOL 200CX microscope fitted with an eucentric goniometer ($\pm$ 60°), and the high resolution electron microscopy (HREM) images were recorded with a TOPCON 02B operating at 200 kV and having a point resolution of 1.8 Å (spherical abberation constant, Cs = 0.4 mm). The actual cation ratio was determined from energy dispersive spectroscopy (EDS) analyses carried out on numerous crystallites. Powder X-ray diffraction data were collected using XpertPro Philips diffractometer equipped with a secondary graphite monochromator and working with the Cu Kα radiation. Data collection was carried out by continuous scanning (step = 0.02° (2θ), preset = 10 s) over an angular range $10° \leqslant 2\theta \leqslant 120°$. The data were refined by profile analysis with the program Fullprof (version 1.5 included in the Winplotr package).[19]

Magnetic properties were studied by means of a Quantum Design SQUID magnetometer and resistivity has been obtained from resistance measurements (four-probe technique) performed with a Quantum Design Physical Properties Measurements System. The same set-up was also used for thermopower method (steady-state method).

III. Results

III.1. Structural study

With the above experimental conditions, a nearly pure phase with nominal composition $Tl_{0.5}Sr_{2.5}CoO_{4.88}$ was isolated. The EDS analysis carried out on numerous fragments of crystals confirms this cationic composition, *i.e.* $Tl_{0.42}Sr_{2.48}Co_{1.1}$, while the chemical analysis, using redox titration, shows an oxygen deficiency $\delta \approx 0.2$–0.25. Note that the cationic composition remains the same for all the analysed microcrystals. The X-ray powder diffraction (XRPD) data of the as-synthesized $Tl_{0.4}Sr_{2.5}Co_{1.1}O_{4.8}$ (Fig. 1b) reveals close structural relationships with the $TlSr_2CoO_5$ cobaltite (Fig. 1a). Both structures exhibit the same tetragonal 1201-type subcell: $a = b \approx a_p$ and $c \approx c_{1201} \approx 9$ Å. Nevertheless a significant difference can be observed between the two data sets, leading to different cell parameters (Table 1) and suggesting a possible symmetry change. In order to check the last hypothesis, a TEM study coupled with EDS analyses was carried out.

Average structure. The ED observations allow the reciprocal space to be reconstructed by tilting around the main crystallographic axes. The characteristic $[001]_p$, $[010]_p$ and $[110]_p$ oriented patterns are shown in Fig. 2. They exhibit a set of intense reflections, related to the 1201 subcell, associated with sharp extra weak reflections (white arrows in Fig. 2b) that lead to an orthorhombic B-type supercell with $a_s \approx 2a_{1201} \approx 2a_p$, $b_s \approx a_{1201} \approx a_p$ and $c_s \approx 2c_{1201}$ (a_p is the parameter of the ideal perovskite unit cell and the suffix s refers to the orthorhombic supercell). The determination of the conditions limiting reflections is difficult due to the coexistence of nanodomains, as further detailed. The observed conditions *hkl*: $h + l = 2n$ are compatible with $B22_12$, $B222$, $Bm2m$, $Bmm2$ and $Bmmm$ as possible space groups. Different hypotheses can be put forward for explaining the actual superstructure, the two most probable being a Tl(Co)/Sr cation ordering at the level of the intermediate layer, similarly to the Bi-based 1201-type cobaltites,[16] and/or an oxygen/vacancy ordering. HREM can provide two important pieces of information for understanding the phenomenon, namely the nature of the atomic layers, which are mainly involved in the structural mechanism, and its extent in the bulk.

The HREM study has been carried out, selecting especially the $[\mathbf{110}]_p$ and $[\mathbf{100}]_p$ viewing directions. They correspond, respectively, to the $[\mathbf{210}]_s$ and $[\mathbf{2\bar{1}0}]_s$ directions of the orthorhombic supercell, for the former, and to the $[\mathbf{100}]_s$ and $[\mathbf{010}]_s$ directions of the orthorhombic supercell, for the latter. The $[\mathbf{110}]_p$ images exhibit a highly regular contrast, which allows the assertion that viewed along that direction there is

Table 1 Structural data refined in 1201 subcell of $TlSr_2CoO_5$ and $Tl_{0.4}Sr_{2.5}Co_{1.1}O_{5-\delta}$ cobaltites

		$TlSr_2CoO_5$[18]					$Tl_{0.4}Sr_{2.5}Co_{1.1}O_{4.75}$ as-synthesized					$Tl_{0.4}Sr_{2.5}Co_{1.1}O_5$ oxygen annealed				
Atom	Site	*X*	*Y*	*Z*	*B*/Å^2	*n*	*X*	*Y*	*Z*	*B*/Å^2	*n*	*X*	*Y*	*Z*	*B*/Å^2	*n*
Tl	1a	0	0	0	0.15	0.93(5)	0.069(2)	0	0	0.9(1)	0.38(1)	0.063(3)	0	0	0.7(2)	0.39(1)
Sr(1)	1a						0.069(2)	0	0	0.9(1)	0.62(1)	0.063(3)	0	0	0.7(2)	0.61(1)
Sr(2)	2h	1/2	1/2	0.2903	0.15	2	1/2	1/2	0.2894(2)	0.34(5)	2	1/2	1/2	0.2949(2)	0.0(1)	2
Co	1b	0	0	1/2	0.15	1	0	0	1/2	0.5(1)	1	0	0	1/2	0.6(1)	1
O(1)	1c	1/2	1/2	0	0.15	1	1/2	1/2	0	1.5(1)	1	1/2	1/2	0	1.2(2)	1
O(2)	2g	0	0	0.232(3)	0.15	2	0	0	0.252(1)	1.5(1)	2	0	0	0.253(1)	1.2(2)	2
O(3)	2e	0	1/2	1/2	0.15	2	0	1/2	1/2	1.5(1)	1.75(5)	0	1/2	1/2	1.2(2)	2.10(5)
Cell parameters (*P4*/*mmm*)		a = 3.7571(1) Å c = 8.7920(2) Å (T = 373 K)					a = 3.7408(1) Å c = 9.0925(1) Å (T = 293 K)					a = 3.7560(1) Å c = 9.0217(1) Å (T = 293 K)				

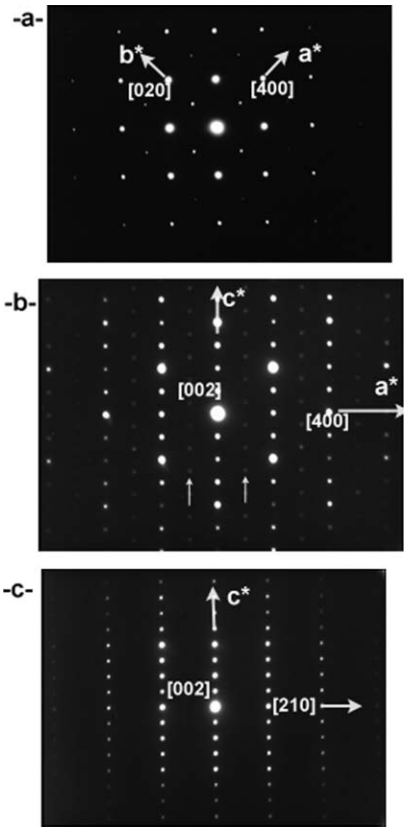

Fig. 2 Experimental ED patterns oriented (a) $[001]_s$, (b) $[010]_s$ and (c) $[\bar{1}0]_s$. The patterns are indexed in the $2a_p \times a_p \times 2c_{1201}$ superlattice.

no signature of any ordering features, even at a short range level. This is illustrated in Fig. 3 where the cation positions are imaged as bright dots.

The 1201-type stacking mode of the layers is clearly identified along $[100]_p$. One example is given in Fig. 4, recorded for a focus value where the high electron density zones are highlighted. Three adjacent rows of the brighter staggered dots are correlated to the cations of the $[AO]_\infty$ layers ; they are separated by a single row of gray dots, associated with the $[CoO_{2-\delta}]_\infty$ layer. The experimental $[100]_p$ and $[110]_p$ images through focus series confirm the classical 1201-type stacking mode of the layers; which are in agreement with the HREM studies of other 1201-type compounds. Moreover, the investigation of numerous grains showed the high regularity of the periodicity along the *c*-axis and the absence of a stacking fault.

Local ordering. Deviations from the homogeneous contrasts of the well-known 1201-structures are observed when viewing the crystals along $[010]_s$. They mainly appear in the form of local modulation of the intensity and small displacements of

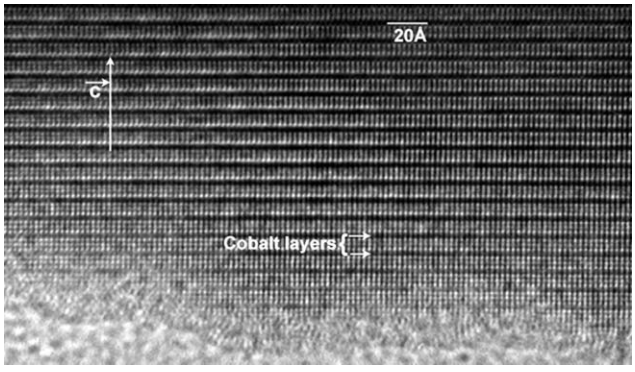

Fig. 3 Experimental $[110]_p$ HREM image. Tl and Sr positions are imaged as bright dots.

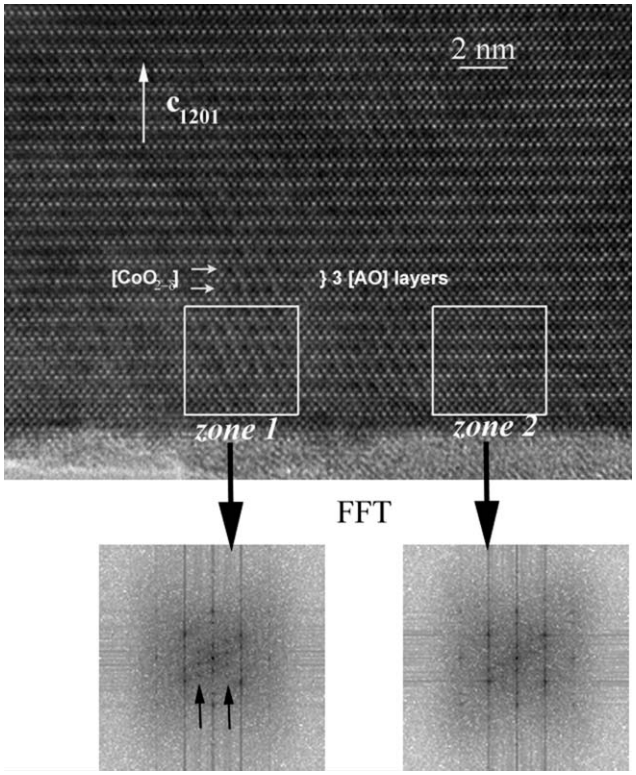

Fig. 4 Experimental $[100]_p$ HREM images. Ordered and non-ordered zones are labelled 1 and 2, respectively. Corresponding FFT are inserted.

the bright and/or gray dots with regard to the expected regular spacing. One example is shown in Fig. 4, comparing the zones denoted 1 and 2. The local EDS analyses showed that there is no significant deviation between these zones. In zone 1, small displacements at the level of the $[CoO_{2-\delta}]_\infty$ layers are observed along $[100]_s$ as gray dots alternately moved closer and further away forming pairs separated by larger dark dots. Note that the effect is shifted by $a_p/2$ in the adjacent Co layers. In zone 2, the spacing and intensity are uniform. The fast Fourier transform (FFT) calculated for these two zones, confirm the appearance of extra reflections in zone 1, in a centered arrangement (black arrows in Fig. 4) involving the parameters $2a_p \times 2c_{1201}$. This is in agreement with the experimental $[010]_s$ ED pattern (Fig. 2b) of the B-type supercell. On the contrary, in zone 2, there is no extra reflection in the FFT, in agreement with the regular contrast. In that case, two simple hypotheses can be first put forward, namely either a $[100]_s$ orientation of the zone or a $[100]_p$ orientation of a classical non-modulated cell. This point will be discussed further.

Experimental images of the ordered area are enlarged in Fig. 5a, for two focus values (estimated as −45 nm and 10 nm) where the cation positions are highlighted. For $\Delta f = -45$ nm, the effect is especially visible at the level of the Co layers, as described above, whereas for $\Delta f = 10$ nm, it is also visible at the level of the SrO layers and results in alternating bright and gray dots with a $2a_p$ periodicity. In both images, the arrangement of the pairs and intensity modulation are shifted by a_p in the neighboring Co and Sr layers.

The images suggest that the superstructure is not induced by long range cation ordering in the mixed layers, in contrast to what is observed between the Bi(Co) and Sr species in the strontium rich $(Bi_{0.5}Sr_{0.5})Sr_2CoO_{5-\delta}$ cobaltites[16] (except possibly in the form of local defects) but rather by an oxygen/vacancy ordering phenomenon. From the observation of Co pairs formation, a model can be proposed based on an oxygen/vacancy ordering in the cobalt layer with the formation of bipyramids Co_2O_{10}. This model is drawn in Fig. 5b. This phase

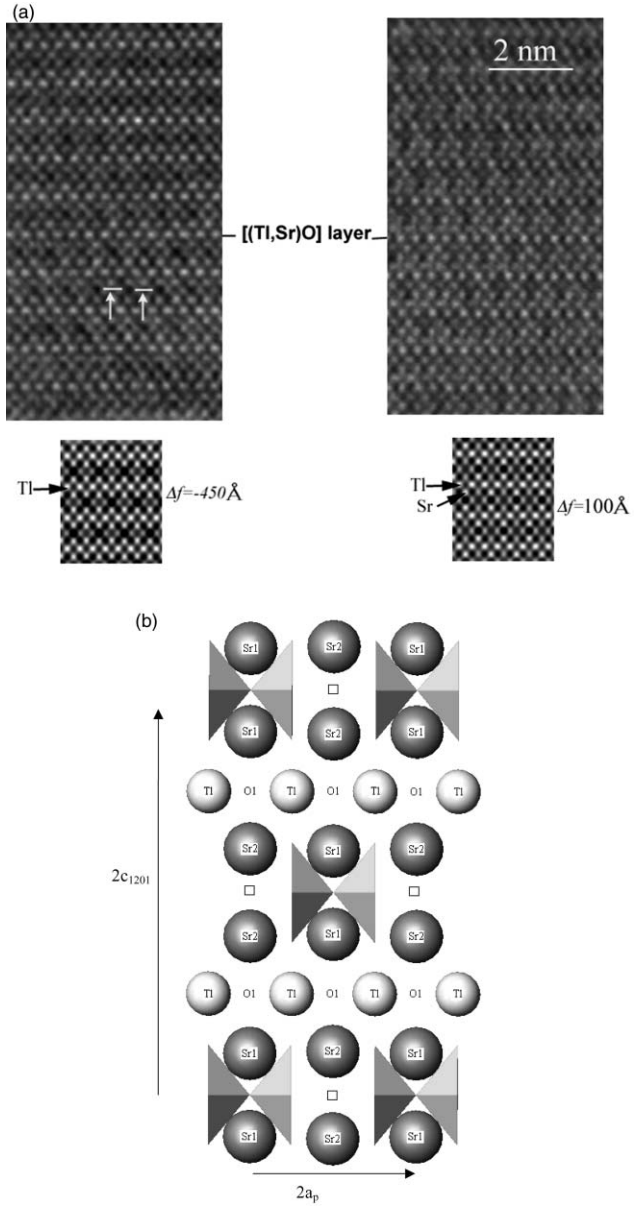

Fig. 5 (a) $[100]_p$ enlarged ordered zone with two different focus values showing modulated contrasts at the level of cobalt layers (white arrows) and [SrO] layers and (b) structural model of the ordered oxygen deficient $Tl_{0.4}Sr_{2.5}Co_{1.1}O_{4.5}$ oxide. Simulated HREM images corresponding to the latter model, calculated for a crystal thickness of 50 Å, are inserted in (a).

is built up from the intergrowth of double $[AO]_\infty$ rock salt type layers $[Sr_{0.5}Tl_{0.4}Co_{0.1}O_2]_\infty$ and $[SrO]_\infty$, with single ordered oxygen deficient perovskite $[SrCoO_{2.5}]_\infty$ layers similar to that of $YBaFeCuO_5$.[20] The face centering of the superstructure $Tl_{0.4}Sr_{2.5}Co_{1.1}O_{4.5}$ is a way to decrease the strains induced by the oxygen vacancies in the framework. The orientation of the pyramids (basal planes parallel to the *c*-axis) could involve a coupled Sr and O displacement.

As above mentioned, the contrasts of this ideal ordered phase $Tl_{0.4}Sr_{2.5}Co_{1.1}O_{4.5}$ are not observed in the whole grain, but only in more or less extended areas, as with the adjacent zones 1 and 2 shown in Fig. 4. From numerous $[\mathbf{100}]_s$ or $[\mathbf{010}]_s$ oriented crystallites studied, it appears that all of them exhibit a patchwork of ordered and non-ordered domains. The first origin of this phenomenon can be correlated to the existence of $[\mathbf{100}]_s$ and $[\mathbf{010}]_s$ oriented domains. These oriented domains can be easily explained by the pseudo-tetragonal character of the subcell, the oxygen vacancies running along one of the two equivalent $[\mathbf{100}]_p$ directions, the small size of the domains explaining the problems met during the ED study. However, in such a rather classical case of twinning domains, one could expect that the extent of the $[\mathbf{100}]_s$ and $[\mathbf{010}]_s$ oriented areas, estimated from numerous observations, is statistically equivalent. The extent of non-ordered domains (associated with $[\mathbf{100}]_s$ domains) appears to be significantly more important than that of the ordered zones, suggesting a second origin of the patchwork: there also exist domains without any superstructure, likely tetragonal. This tetragonal phase is supposed to be fully oxygenated with perovskite layers built of octahedra.

As a conclusion, the ED and HREM study showed that in the as-synthesized sample, the oxygen vacancies are not randomly distributed but are locally ordered in more or less extended areas ranging from a few to a few hundred nanometers. This can be described by the coexistence of two limit phasoïds, a stoichiometric $Tl_{0.4}Sr_{2.5}Co_{1.1}O_5$ with cobalt octahedra and an ordered oxygen deficient one $Tl_{0.4}Sr_{2.5}Co_{1.1}O_{4.5}$ with cobalt pyramids, as a result of the actual oxygen content of the sample, close to 4.7–4.8, and also the thermal process, especially the rather rapid decrease of the temperature, which would favor the disproportionation between those phasoïds.

X-ray analysis. In order to test the validity of this model and to check the position of the oxygen vacancies, an X-ray diffraction data study was carried out. First the refinements of the structure were performed starting from the parameters of the basic 1201 cobaltite structure[18] (see Table 1). In this way, the partial substitution of thallium for strontium is confirmed, illustrated by the increasing of the stacking parameter (c = 9.10 Å in the Tl/Sr-1201 phase instead of c = 8.8 Å in pure Tl-1201 phase[18]). Indeed oxygen deficiency is detected at the level of cobalt layers and from these calculations the global oxygen content can be estimated as close to 4.8, in agreement with the chemical analyses. At this stage, the agreement factors R_p = 10.8, R_{wp} = 13.7, R_B = 6.8 and χ_i^2 = 2.09 have been obtained. Taking into account the previous TEM analyses and the proposed structural model, the subcell parameters can be extrapolated to a possible *Bm*2*m* supercell ($2a_p \times a_p \times 2c_{1201}$) by considering ordered oxygen vacancies at the level of $[CoO_{1.8}]$ layers (Table 2). Nevertheless the refinements of this set of second structural parameters were not conclusive since the corresponding reliability factors are slightly higher than those obtained in the basic 1201 lattice. This point corroborates the comparison of XRD data (Fig. 1) between the stoichiometric (*P*4/*mmm*) and strontium-rich 1201-type cobaltites, which has not revealed any significant extra reflections or the nanostructural observations that evidence the coexistence of two randomly distributed phasoïds. However, these extrapolated positions, corresponding to the $Tl_{0.4}Sr_{2.5}Co_{1.1}O_{4.5}$

Table 2 Atomic positions of as-prepared $Tl_{0.4}Sr_{2.5}Co_{1.1}O_{4.8}$ refined in the actual *Bm*2*m* superlattice

Atom	Site	*X*	*Y*	*Z*	B_{iso}/Å^2	*n*
Tl(Co)	4c	0.2180(9)	0.5	0.25	1.3(1)	1.89(2)
Sr	4c	0.25	0.5	0.25	1.4(4)	2.11(2)
Sr(1)	4d	0	0	0.1028(3)	0.39(5)	4
Sr(2)	4d	0.5	0	0.1079(3)	0.39(5)	4
Co	4e	0.25	0.5	0	1.6(1)	4
O(1)	2d	0	0	0.25	0.51(5)	4
O(2)	8f	0.25	0.5	0.1242(6)	0.51(5)	8
O(3)	4e	0.25	0	0	0.9(3)	4
O(4)	2b	0.5	0.5	0	0.9(3)	2
O(5)	2a	0	0.5	0	0.9(3)	1.2(2)[a]

Cell parameters/Å a = 7.4812(5); b = 3.7410(2); c = 18.1849(2)

[a] $n_{O(5)}$ = 0 in the ideal model of ordered oxygen deficient $Tl_{0.4}Sr_{2.5}Co_{1.1}O_{4.5}$.

phasoïd, have allowed a simulation of the contrast images. These calculated images (Fig. 5a) fit well the experimental ones shown in Fig. 4, especially the displacements in the $[SrO]_\infty$ layers *versus* thickness and defocus values.

Annealed samples. In order to support the above structural study of this cobaltite, and especially the issue of oxygen non-stoichiometry, the sample was annealed. One part of the as-synthesized bars was annealed under an oxygen pressure of 150 bar at 400 °C for 48 h and the other part under a reducing atmosphere (Ar/H_2 flow at 300 °C for 12 h) The crystal nanostructure of the annealed phases has been checked by TEM techniques. The ED patterns of the reduced sample are similar to those of the as-synthesized phase and the reconstruction of the reciprocal space has evidenced the B-type supercell. The direct and simple comparison of the relative intensity of the extra reflections can hardly be made due to the strong interactions between the electrons and the material induced by numerous domains. However, the HREM images show clearly that the average size of the domains is significantly larger. This effect is interpreted as the extent of the ordered phase correlated to a loss of oxygen. The electron diffraction investigation of the oxidized sample showed also that the intense Bragg reflections of the 1201-type structure are retained after annealing. However, the system of extra reflections is modified. In that case, the extra reflections characteristic of the orthorhombic supercell are significantly less intense, sometimes scarcely visible or really absent. Moreover, the sharpness of the peaks has disappeared, replaced by diffuse spots elongated along $[\boldsymbol{hk0}]^*$. One example is given in Fig. 6a. The HREM study confirmed that the extent of the ordered oxygen deficient phase $Tl_{0.4}Sr_{2.5}Co_{1.1}O_{4.5}$ was considerably reduced, and even entirely absent in some crystallites. One example is given in Fig. 6b. It also explained the elongated and streaky spots in the ED patterns, generated by the formation of tiny domains with a new periodicity, for instance $3a_p$ as illustrated by the white arrows in Fig. 6b. In parallel to the TEM observations, the XRD data were also refined in the common subcell *P4/mmm* and the results are compared (Table 1) to those obtained for the as-synthesized sample and the stoichiometric $TlSr_2CoO_5$ oxide.[18] A significant decrease of the *c* parameter was observed from the as-synthesized to the oxidized sample

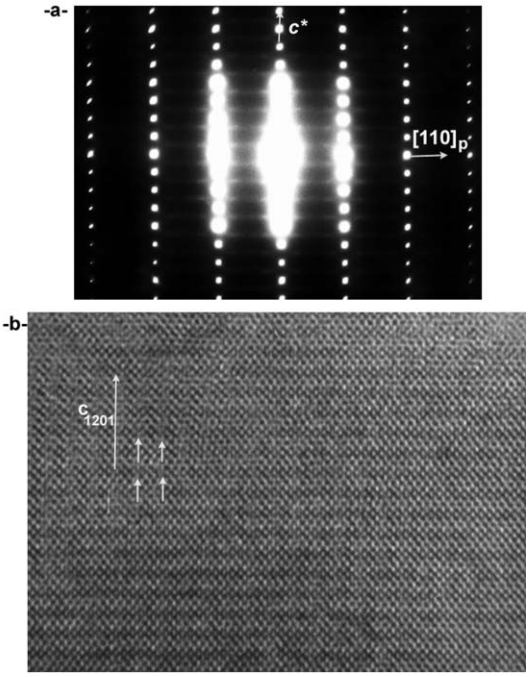

Fig. 6 Experimental (a) $[\bar{1}0]_p$ ED pattern and (b) $[100]_p$ HREM image of the oxygen pressure annealed (Tl, Sr)-1201.

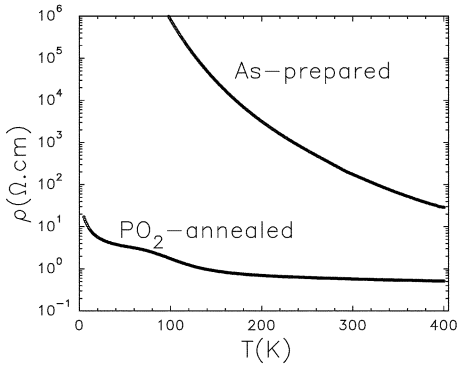

Fig. 7 *T* dependence of resistivity (ρ) for the Sr-rich Tl-1201 phase, as-prepared and post-annealed in oxygen pressure (PO_2).

while the refinements of occupancy factors led to the average formula $Tl_{0.4}Sr_{2.6}CoO_5$ with the oxygen sites at the level cobalt layers almost fully occupied. This structural evolution can be compared to the results reported in the case of the oxygen dependent series $(Bi_{0.4}Sr_{0.45}Co_{0.15})Sr_2CoO_{5-\delta}$[16] where the same behavior was observed when the global oxygen content increased. So, even if the oxygen content could not be determined with accuracy, we can conclude that the global oxygen content of the oxidized sample increased.

III.2. Magnetic and transport properties

In contrast to $TlSr_2CoO_5$ which exhibits a M-I transition at 300 K[14,15] the as-prepared $Tl_{0.4}Sr_{2.5}Co_{1.1}O_{5-\delta}$ 1201 cobaltite is characterized by a semiconducting-like behavior from 400 K down to $T \sim 100$ K, which corresponds to the maximum resistance ($\sim 10^6$ Ω) measurable with our set-up (Fig. 7). In addition, its resistivity is 100 times larger at 360 K, (4 Ω cm) compared to $TlSr_2CoO_5$ (4.10^{-2} Ω cm). Since in $TlSr_2CoO_5$, the M-I is connected to an anomaly in the magnetic susceptibility at T_{MI}, no magnetic transition is expected in the cobaltite under study. This is illustrated by the *T* dependent inverse susceptibility which follows a Curie–Weiss law from 50 K to 400 K (curve a in Fig. 8) indicating a lack of magnetic transition in this *T* range. By fitting the expression $\chi = C/(T - \theta_p)$ to the data one deduces an effective paramagnetic moment of $\mu_{eff} = 3.43\mu_B$ from the Curie constant and $\theta_p = -160$ K for the paramagnetic temperature. The latter negative value of θ_p, indicative of antiferromagnetic correlations, contrasts with the positive value ($\theta_p = 200$ K) observed for $TlSr_2CoO_5$.[14] The μ_{eff} value can be obtained by considering a mixture of 0.2 high spin (H.S.) Co^{3+} and 0.9 intermediate spin (I.S.) Co^{3+} , in agreement with the chemical analysis $Tl_{0.4}Sr_{2.5}Co_{1.1}O_{4.8}$ implying that cobalt is mainly trivalent. As shown in the structural part, the oxygen vacancies can be partly refilled by oxygen pressure annealing. Interestingly, this strongly affects the transport

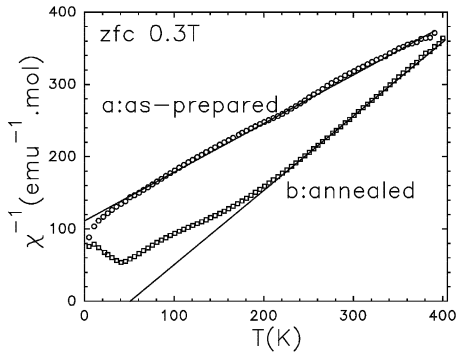

Fig. 8 *T* dependent inverse magnetic susceptibility (χ^{-1}) for the as-prepared (a) and post-annealed (b) Sr-rich 1201 phase. The lines correspond to the Curie–Weiss fitting.

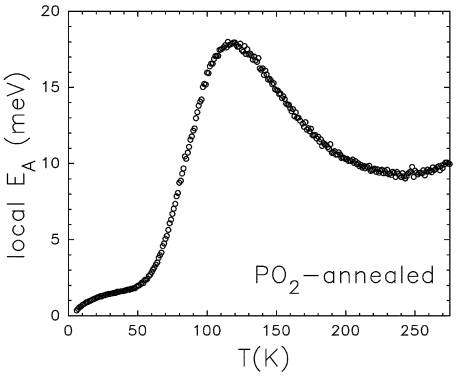

Fig. 9 T dependent local activation energy of the O_2 annealed sample.

properties as shown in Fig. 7. At 300 K, ρ shifts down from 20 Ω cm for the as-prepared to 5×10^{-2} Ω cm for PO_2 annealed cobaltite. This $\rho_{300\ K}$ value is more comparable to that of $TlSr_2CoO_5$,[14] $\sim 3 \times 10^{-2}$ Ω cm in the high temperature metallic state. In spite of the similarity of its high temperature resistivity to $TlSr_2CoO_5$, the annealed, strontium-rich 1201 cobaltite does not exhibit an abrupt M-I transition at ~300 K as in the pure Tl-1201. The resistivity is only weakly dependent on T in the range 400–150 K and then ρ shows a tendency towards localization. This is more clearly visible in Fig. 9 where the local activation energy $E_A^{local} = k \times (d\ln\rho)/(dT^{-1})$ (k is the Boltzmann constant) is plotted as a function of temperature. First the low E_A values, $E_A < 20$ meV, show that this sample does not behave as a true semiconductor in this T range. Second, after the E_A increase from 220 to 120 K, E_A decreases below 120 K, which is indicative of a slowing down of the localization process. When compared with the magnetic susceptibility (curve b in Fig. 8), one could attribute the increase of E_A below ~220 K to the downward deviation from the linearity of $\chi^{-1}(T)$ below this temperature. This effect can be either due to long-range antiferromagnetic interactions or to a change in the spin state of cobalt. However, since the slope below 200 K is lower than above it, the spin state would become higher as T decreases to explain the larger μ_{eff} value, which has no physical meaning. Moreover, from the linear fitting of $\chi^{-1}(T)$ in between 200 and 400 K, one obtains $\mu_{eff} = 2.78\mu_B$ per cobalt, *i.e.* very close to the value expected for I.S. Co^{3+} ($S = 1$), $\mu_{eff} = 2.83\ \mu_B$. According to the structural study, which shows an increase of oxygen content under PO_2 annealing, a part of the Co species become tetravalent. In the $LaCoO_3$ perovskite, the creation of holes by aliovalent La^{3+}/Sr^{2+} substitutions tends to be in the form of low spin (L.S.) Co^{4+} ($t_{2g}^5e_g^0$) with $\mu_{eff} = 1.73\mu_B$.[2] A mixture of 0.2 L.S. Co^{4+} with 0.8 I.S. Co^{3+} yields $\mu_{eff} = 2.83\mu_B$ but the same μ_{eff} value could also be obtained with more L.S. Co^{4+} compensated by the creation of H.S. Co^{3+} ($\mu_{eff} = 4.9\ \mu_B$). In fact, $\rho(T)$ curves of the as-prepared and annealed samples cannot be simply described by a semiconducting behavior (Arrhenius law) as shown by the absence of linearity in the $\log(\rho)$ *versus* T^{-1} plots shown in Fig. 10. According to the localizing behavior observed for the as-prepared sample probably linked to the large disorder induced by oxygen vacancies on the Co–O network, the $\rho(T)$ curve can be fitted by a variable range hopping model as shown from the linear $\rho(T^{-1/4})$ plot of Fig. 11. In contrast, the less oxygen-deficient CoO_3 array in the PO_2 annealed sample makes charge delocalization easier, which explains the lower resistivity (Fig. 7). Since in addition the degree of disordering in the layer has decreased, the $\rho(T)$ curve cannot be described by a variable range hopping law (Fig. 11). According to the small values of the local activation energy (Fig. 9), a small polarons model is more correct if one refers to the linear ρ/T *versus* T^{-1} curve in Fig. 12, which satisfies the predicted expression $\rho = A \times T \times \exp(W/kT)$,

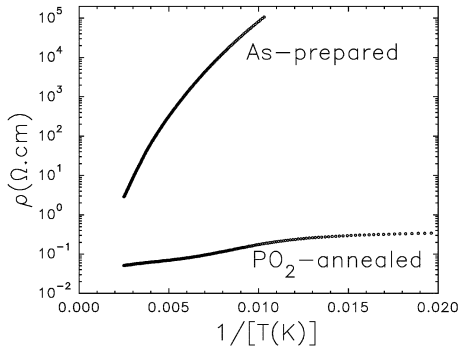

Fig. 10 T^{-1} dependence of ρ for both samples showing the lack of linearity.

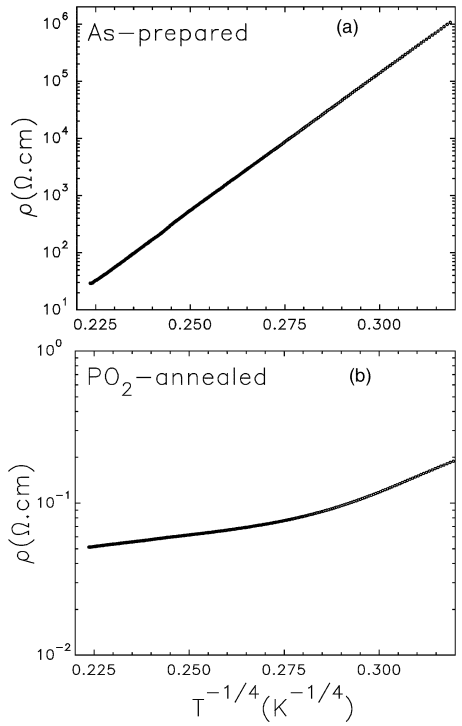

Fig. 11 $T^{-1/4}$ dependence of ρ for (a) the as-prepared and (b) the oxygen annealed samples.

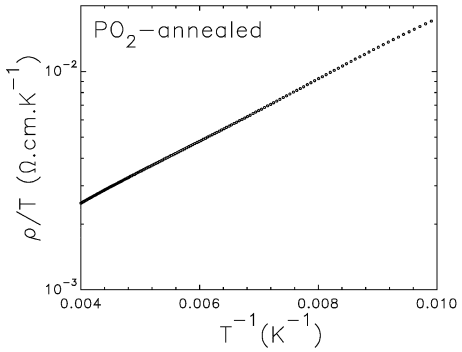

Fig. 12 T^{-1} dependence of ρ/T for the oxygen annealed Tl/Sr-1201 phase.

where A is a constant and W represents the hopping energy. This difference in the transport properties as the oxygen content increases is also reflected in the magnetic behavior. The positive $\theta_p = +50$ K value for the PO_2 samples contrasts with the negative $\theta_p = -160$ K for the as-prepared one (Fig. 8). In the former (Fig. 8b), the dominant magnetic correlations at high temperature are ferromagnetic. The existence of an irreversibility in the field-cooling (fc) and zero-field-cooling

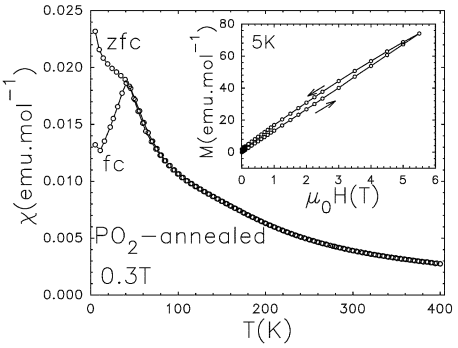

Fig. 13 *T* dependent magnetic susceptibility for the oxygen annealed sample. Data are collected after zero-field-cooling (zfc) and after field-cooling (fc) processes. Inset: Isothermal ($T = 5$ K) field dependent (H) magnetization (M) curve of the PO_2 annealed 1201 phase.

(zfc) $\chi(T)$ curves (Fig. 13) attests that ferromagnetic regions develop at low T, the zfc branch showing a cusp-like shape. However, from the field-dependent magnetization curve registered at 5 K only a small ferromagnetic component is observed with a complete absence of saturation even at 5 T and a small remnant value (inset of Fig. 13). This weak ferromagnetic behavior at low T is probably responsible for the decrease in local activation energy starting below 120 K in Fig. 9. Ferromagnetic clusters can be created in the hole-rich region: rules for 180° superexchange interactions predict a ferromagnetic behavior between e_g^0 (Co^{4+} H.S.) and e_g^1 (Co^{3+} I.S.).[2] These interactions may explain the decrease in $\chi^{-1}(T)$ below about 200 K.

It appears thus that the changes in the oxygen content induced by oxygen pressure annealing strongly affect the transport properties ($\rho_{100\ K}$ is 10^6 times lower in the PO_2 sample than in the as-prepared one) and to a lesser extent the magnetic properties. As mentioned in the introduction, some metallic cobaltites such as $NaCo_2O_4$ exhibit interesting large thermopower values at room temperature ($S \sim 100\ \mu V\ K^{-1}$) which makes them promising candidates for application.[10] However, as shown in Fig. 14, the thermopower of the (Tl/Sr)-1201 cobaltite is very sensitive to the oxygen content : $S_{300\ K}$ decreases from $+50\ \mu V\ K^{-1}$ to $+18\ \mu V\ K^{-1}$ as the oxygen content increases. As for the perovskite, the most conducting (Tl,Sr-1201) sample therefore exhibits a too low-temperature thermoelectric power (TEP) value for applications. This emphasizes that the unique TEP properties of metallic $NaCo_2O_4$[10,11] and misfit cobaltites[12] lie in the peculiar structure of their CoO_2 layers made of edge-shared CoO_6 octahedra. In contrast, in the $La_{1-x}Sr_xCoO_3$ perovskite, as the samples become metallic by Co^{4+} creation, the TEP value drops to very small absolute values.[2] Nevertheless, the $S(T)$ curve of the PO_2 sample is instructive. It shows first a quasi-T independent TEP value from 300 to 200 K, *i.e.* in the T region where the $\rho(T)$ curve is almost flat and where the sample's magnetic state is

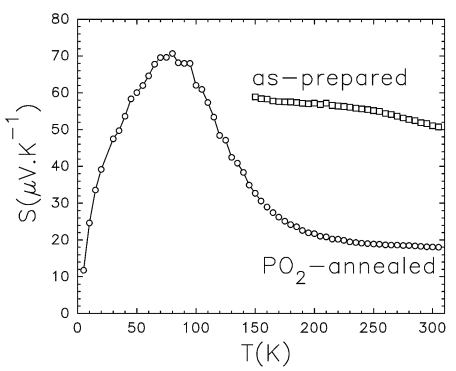

Fig. 14 *T* dependent thermoelectric power (S).

paramagnetic according to the linear $\chi^{-1}(T)$ curve. There is then a clear change in the electronic properties with a progressive S increases as T decreases from 200 to 75 K, where S reaches a maximum ($S = +65\ \mu V\ K^{-1}$). It should be pointed out that the $TlSr_2CoO_5$ cobaltite also exhibits an $S(T)$ curve with a maximum ($S = +200\ \mu V\ K^{-1}$ at 150 K) but a negative S value in the metallic state, $\sim -10\ \mu V\ K^{-1}$ at 320 K,[14] against $S = +18\ \mu V\ K^{-1}$ at 300 K in our Sr-rich-1201 cobaltite. These opposite signs could be due to different kinds of spin states. On one hand, the positive TEP value in the Sr-rich 1201 phase would indicate that the majority of carriers are Co^{4+} holes in the I.S. Co^{3+} matrix, the concentration of the former increasing under annealing if one compares the obtained S decrease with the results of $La_{1-x}Sr_xCoO_3$ holes doped cobaltite.[2] On the other hand, although the $TlSr_2CoO_5$ phase also contains Co^{3+} and Co^{4+} species, the cobalt high-spin state of the high temperature structural form would explain metallicity *via* a $\sigma^{*2}_{x^2-y^2}$ less than half-filled band implying electron doping.[14]

IV. Conclusions

This work demonstrates that the formation of mixed strontium based rock salt type layers, shown recently in the Bi–Sr–Co–O system,[16] can be enlarged to thallium based systems. In this way, a new form of 1201-type cobaltite, $(Tl_{0.4}Sr_{0.5}Co_{0.1})Sr_2CoO_{4.8}$, has been isolated. As well as the mixed [(Tl,Co,Sr)O] layers, this oxide differs from the parent stoichiometric $TlSr_2CoO_5$ phase[18] by the presence of oxygen vacancies. From HREM observations, this sample can be described as a patchwork of two phasoïds, an oxygen stoichiometric one $(Tl_{0.4}Sr_{0.5}Co_{0.1})Sr_2CoO_5$, and an ordered oxygen deficient one, $(Tl_{0.4}Sr_{0.5}Co_{0.1})Sr_2CoO_{4.5}$. However, complementary syntheses are in progress to understand the behavior of this sample *versus* thermal treatment and atmosphere, and to minimize the oriented domains in order to refine with accuracy the superstructure $2a_p \times a_p \times 2c_{1201}$ of this new ordered oxygen deficient cobaltite. The great sensitivity of both the magnetic and transport properties to the oxygen content shows that this phase lies close to a M-I transition. From the electronic transport properties, it appears that the (Tl,Sr)-1201 phase is hole-doped with Co^{4+} carriers in a Co^{3+} matrix. This behavior is rather similar to that of the $La_{1-x}Sr_xCoO_3$ perovskite but contrasts with that of the stoichiometric $TlSr_2CoO_5$ phase, which exhibits a negative thermopower value in the metallic state. This emphasizes the richness of the structural and physical properties of cobaltites.

References

1 P. M. Raccah and J. B. Goodenough, *Phys. Rev.*, 1967, **155**, 932.
2 M. A. Senaris-Rodriguez and J. B. Goodenough, *J. Solid State Chem.*, 1995, **118**, 323.
3 S. Yamaguchi, H. Tamiguchi, H. Takagi, T. Arima and Y. Tokura, *J. Phys. Soc. Jpn.*, 1995, **54**, 1885.
4 R. Mahendiran, A. K. Raychaudhuri, A. Chaimini and D. D. Sarma, *J. Phys.: Condens. Matter.*, 1995, **7**, L561.
5 H. Fjellvag, E. Gulbrandsen, S. Aasland, A. Olsen and B. Hauback, *J. Solid State Chem.*, 1996, **124**, 190.
6 S. Aasland, H. Fjellvag and B. Hauback, *Solid State Commun.*, 1997, **101**, 187.
7 H. Kageyama, K. Yoshimura, K. Kosuge, H. Mitamura and T. Goto, *J. Phys. Soc. Jpn.*, 1997, **66**, 1607.
8 A. Maignan, C. Michel, A. C. Masset, C. Martin and B. Raveau, *Eur. Phys. J. B*, 2000, **15**, 15657.
9 M. Von Jansen and R. Hoppe, *Z. Anorg. Allg. Chem.*, 1974, **408**, 104.
10 I. Terasaki, Y. Sasago and K. Uchinokura, *Phys. Rev. B*, 1997, **56**, R12685.
11 T. Itoh and I. Terasaki, *Jpn. J. Appl. Phys.*, 2000, **39**, 6658.
12 A. C. Masset, C. Michel, A. Maignan, M. Hervieu, O. Toulemonde, F. Studer and B. Raveau, *Phys. Rev. B*, 2000, **62**, 166.

13 C. Martin, A. Maignan, D. Pelloquin, N. Nguyen and B. Raveau, *Appl. Phys. Lett.*, 1997, **71**, 1421.
14 M. Coutanceau, P. Dordor, J. P. Doumerc, J. C. Grenier, P. Maestro, M. Pouchard, D. Semidubsky and T. Seguelong, *Solid State Commun.*, 1995, **96**, 569.
15 M. Coutanceau, Ph.D. Thesis, Université de Bordeaux I, 1996.
16 A. C. Masset, O. Toulemonde, D. Pelloquin, E. Suard, A. Maignan, F. Studer, M. Hervieu and C. Michel, *Int. J. Inorg. Mater.*, 2000, **2**, 687.
17 M. Coutanceau, J. P. Doumerc, J. C. Grenier, P. Maestro, M. Pouchard and T. Seguelong, *C. R. Acad. Sci. Paris*, 1995, **320**, 675.
18 J. P. Doumerc, M. Coutanceau, A. Demourgues, E. Elkaim, J. C. Grenier and M. Pouchard, *J. Mater. Chem.*, 2001, **11**, 78.
19 J. Rodriguez-Carvajal, in *Collected abstracts of powder diffraction meeting, Toulouse, France*, ed. J. Galy, 1990, p. 127.
20 L. Er-rakho, C. Michel, P. Lacorre and B. Raveau, *J. Solid State Chem.*, 1988, **73**, 531.